On the kinematics and resolution of spectrometers for neutron Brillouin scattering

R. A. Robinson
Los Alamos Neutron Scattering Center
Los Alamos National Laboratory
Los Alamos, New Mexico 87545
USA

ABSTRACT: Neutron Brillouin scattering involves measurement of excitations at smaller Q values than is currently customary. We outline the kinematic constraints on scattering angle and incident energy for excitations with both linear dispersion (sound waves) and parabolic dispersion (ferromagnetic spin waves), and discuss the resolution characteristics of the chopper spectrometer proposed for LANSCE which should be suitable for such studies. In particular, we demonstrate that longitudinal resolution focussing can be exploited both in neutron energy gain and in neutron energy loss.

1. Introduction

In general, measurements of sound velocity by means of inelastic neutron scattering have been made in higher-order Brillouin zones (i.e., not at the reciprocal-space origin) of single crystals using reactor triple-axis spectrometers[1]. If single crystals are unavailable, this method cannot be used. Nor can it be used for amorphous solids, liquids or gases, in which there is no translational symmetry and hence no reciprocal lattice. In these cases, it is necessary to work close to the wave-vector space origin, in a manner analogous to conventional optical Brillouin scattering. Some measurements of this type have been made on triple-axis spectrometers[2] as well as reactor time-of-flight machines[3], but the momentum transfers reached have been relatively large. This necessitates the use of neutron energies rather large in comparison with the energy of the acoustic phonon concerned and very small scattering angles. This is a demanding combination: the use of high neutron energies means that the resolution requirements are tight, while working close to the straight-through beam, and its attendant background will degrade the signal-to-noise ratio of the experiment. However, with the new high-intensity accelerator-based sources such as LANSCE at Los Alamos and ISIS at Rutherford Appleton Laboratory, these experiments should be feasible.

It must be added that the requirement for high incident energies and small scattering angles arises in other areas, for instance, the measurement of highly dispersive spin waves in amorphous magnets[4]. It is the purpose of this article to address the general question of kinematics and resolution for a neutron Brillouin scattering spectrometer and to propose a specific configuration that could be implemented at one of the new high-intensity spallation sources.

For the purpose of discussion, we will consider two sound wave and two magnetic cases: firstly, a material with sound velocity of 1000 ms^{-1} down to a wave-vector Q = 0.05 $Å^{-1}$ and secondly, a material with sound velocity of 6000 ms^{-1} down to Q = 0.3 $Å^{-1}$. The former corresponds loosely to a typical liquid, while the latter corresponds to the longitudinal sound velocity in a fairly hard solid like aluminium, a case that has been considered previously by Reichardt[5] for SNQ. In both of these cases, we will find that one requires scattering angles in the vicinity of 1°. In addition we consider ferromagnets with spin wave stiffnesses D of 30 meVÅ^2 and 300 meVÅ^2. The former of these corresponds loosely to a weak itinerant ferromagnet like Ni_3Al[6], and the latter corresponds loosely to a strong itinerant ferromagnet like iron or nickel[7,8].

An abbreviated version of this work has already appeared elsewhere[9].

2. General kinematical considerations

In general, when designing a spectrometer or deciding how to perform a given experiment, one has some idea of the excitation energy E and the wave-vector Q that one would like to reach. The normal energy and momentum conservation laws for a neutron scattered by an angle ϕ then determine the incident energy E_I that must be used:

$$E_I = \frac{\hbar^2}{4\,m\,\sin^2\phi}\left\{(Q^2 + \varepsilon\sin^2\phi) \pm \cos(\phi)\sqrt{Q^4 - \varepsilon^2\sin^2\phi}\right\} \qquad (1)$$

where

$$\varepsilon = \frac{2\,m\,E}{\hbar^2} \qquad (2)$$

These equations are perfectly general and are not specific to Brillouin scattering or time-of-flight instruments. There are two solutions to eq.(1). However, they are not always both physical. For instance, in the case of elastic scattering ($\varepsilon \rightarrow 0$), the positive root gives

$$E_I = \frac{\hbar^2 Q^2}{2m\,\sin^2\left(\frac{\phi}{2}\right)} \qquad (3)$$

which corresponds to Bragg's Law, while the negative root gives

$$E_I = \frac{\hbar^2 Q^2}{2m\,\cos^2\left(\frac{\phi}{2}\right)} \qquad (4)$$

which is clearly unphysical. In fact, it can be shown that the negative root is unphysical if $|\epsilon| < Q^2$ (see appendices for proof.) This constraint is shown in Fig. 1, along with the dispersion relations for sound waves with v = 1000, 2000 and 6000 ms^{-1}. For any value of Q in the Brillouin scattering regime, one has two solutions and the negative root is to be preferred as it gives the lower incident energy. For ferromagnetic spin waves, with a dispersion relation $E = DQ^2$, there are two solutions if $D > 2m/\hbar^2$ (0.4826 meVÅ^2). As most systems are stiffer than this, again one is in the two-solution regime and the negative root is to be preferred. In other words, although the relative energy changes in Brillouin scattering are small, it is <u>not</u> a small perturbation on Bragg scattering, or one can say that Brillouin scattering is closer to the $\phi \to 0$ limit than the $E \to 0$ limit.

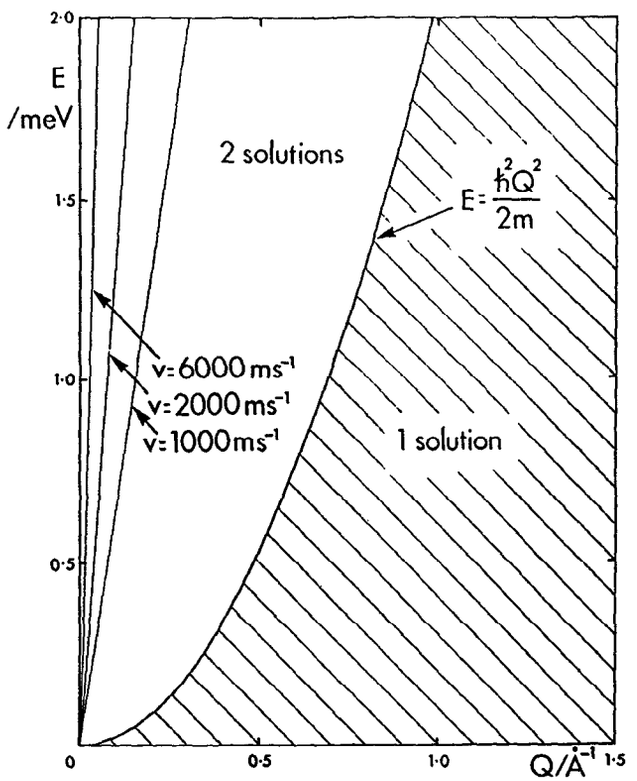

Fig. 1 The region of phase space in which there are two physical solutions to Eq. (1) and in which there is only one. While the high-energy solution is the only one for elastic scattering (E = 0), for any Q-values and sound velocities appropriate for Brillouin scattering, both solutions to Eq. (1) are physical and the low-energy solution is preferred.

For any given E and Q, there is a maximum possible scattering angle ϕ_{max} given by

$$\sin^2\phi_{max} = \frac{Q^4}{\varepsilon^2} \tag{5}$$

and a corresponding incident energy E_I (ϕ_{max}) given by

$$E_I(\phi_{max}) = \frac{\hbar^2}{4m}\left(\frac{\varepsilon^2}{Q^2} + \varepsilon\right) \tag{6}.$$

In addition, there is a minimum possible incident energy $E_{I_{min}}$, corresponding to forward scattering ($\phi = 0$), given by

$$E_{I_{min}} = \frac{\hbar^2}{8mQ^2}(\varepsilon + Q^2)^2 \tag{7}.$$

Equations (5), (6) and (7) serve to define the broad angular and energy range within which one must work for any given value of E and Q.

3. Application to sound waves

For excitations, like sound waves, with a dispersion relation $E = \hbar vQ$, Equations (5), (6) and (7) become

$$\sin^2\phi_{max} = \frac{\hbar^2Q^2}{4m^2v^2} \tag{8},$$

$$E_I(\phi_{max}) = mv^2 + \frac{\hbar vQ}{2} \tag{9}$$

and

$$E_{I_{min}} = \frac{\hbar^2}{8mQ^2}\left\{\frac{2mvQ}{\hbar} + Q^2\right\}^2 \tag{10}.$$

As $Q \to 0$,

$$E_I(\phi_{max}) \to mv^2 \quad \text{and} \quad E_{I_{min}} \to \frac{mv^2}{2} \tag{11}.$$

In other words, the incident energy scale is proportional to v^2 and there is a factor of two available in the choice of E_I, but no more than that.

The variation of E_I with ϕ is shown in Figs. 2 and 3 for sound velocities of 1000 ms^{-1} and 6000 ms^{-1}, respectively.

4. Application to ferromagnetic spin waves

For ferromagnetic spin waves with $E = DQ^2$, Equation (1) can be written in the simplified form

$$E_I = \frac{\hbar^2 Q^2}{4\,m \sin^2\phi}\left\{ 1 + \frac{2mD\sin^2\phi}{\hbar^2} \pm \cos(\phi)\sqrt{1 - \frac{4\,m^2D^2\sin^2\phi}{\hbar^4}} \right\} \tag{12}$$

Clearly, E_I is simply proportional to Q^2 and, as is well known[10], ϕ_{max} is independent of Q:

$$\sin^2\phi_{max} = \frac{\hbar^4}{4\,m^2D^2} \tag{13}.$$

Equations (6) and (7) become

$$E_I(\phi_{max}) = \frac{\hbar^2 Q^2}{4m}\left\{ \frac{4\,m^2D}{\hbar^4} + \frac{2mD}{\hbar^2} \right\} \tag{14}$$

and

$$E_{I_{min}} = \frac{\hbar^2 Q^2}{8m}\left(\frac{2mD}{\hbar^2} + 1 \right)^2 \tag{15}.$$

Note that while the angular range available is independent of Q, the incident energies required for such experiments rise in proportion to Q^2.

The variation of E_I with ϕ is shown in Figs. 4 and 5 for spin wave stiffnesses of 30 meVÅ^2 and 300 meVÅ^2, respectively.

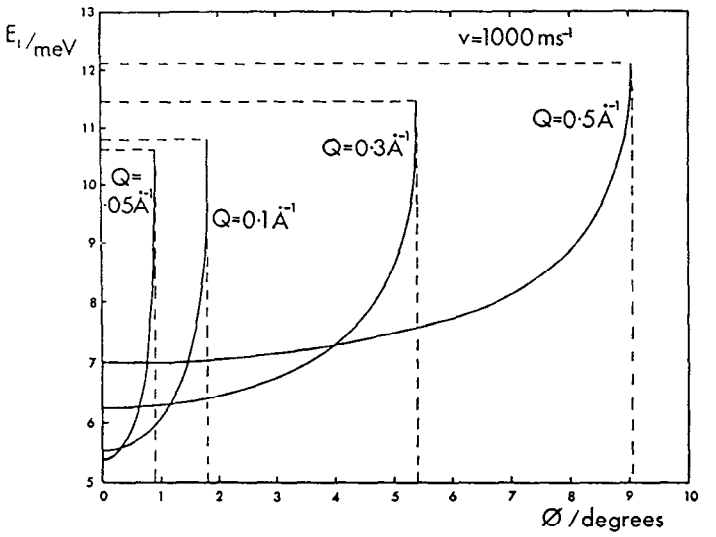

Fig. 2 Plot of Incident energy E_I versus scattering angle ϕ for a sound velocity of 1000 ms^{-1}. The low-energy solution of Eq. (1) is plotted for Q = 0.05, 0.1, 0.3 and 0.5 $Å^{-1}$. The corresponding energies are 0.33, 0.66, 1.97 and 3.29 meV respectively. The dashed lines extend to ϕ_{max} and E_I (ϕ_{max}), respectively. This figure shows the possible trade-off between incident energy and scattering angle for the chosen value of Q and the value of E determined by the choice of Q and v.

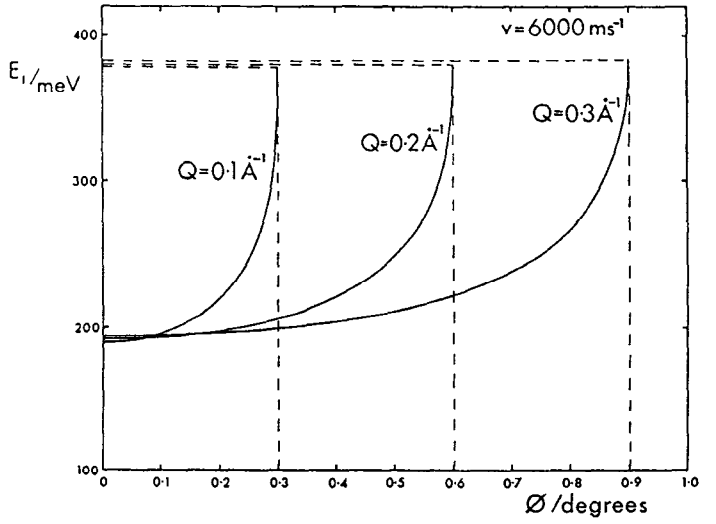

Fig. 3 Plot of incident energy E_I versus scattering angle ϕ for a sound velocity of 6000 ms^{-1}. The low-energy solution of Eqn. 1 is plotted for Q = 0.1, 0.2 and 0.3 $Å^{-1}$. The corresponding energies are 3.95, 7.9 and 11.85 meV, respectively. The dashed lines extend to $\phi_{max}$and E_I (ϕ_{max}) respectively. This figure shows the possible trade-off between incident energy and scattering angle for the chosen value of Q and the value of E determined by the choice of Q and v.

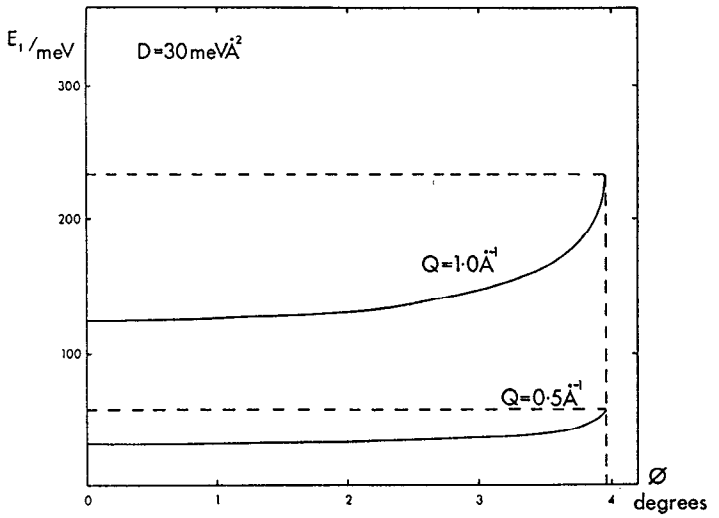

Fig. 4 Plot of incident energy E_I versus scattering angle ϕ for a spin wave stiffness of 30 meVÅ^2. The low-energy solution of Eq. (1) is plotted for Q = 0.5 and 1.0 Å^{-1}. The corresponding energies are 7.5 and 30 meV, respectively. The dashed lines extend to ϕ_{max} and E_I (ϕ_{max}), respectively. This figure shows the possible trade-off between incident energy and scattering angle for the chosen value of Q and the value of E determined by the choice of Q and D.

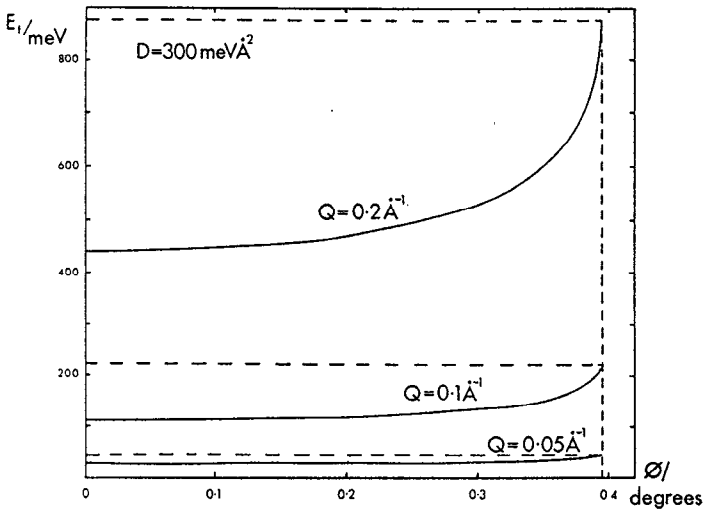

Fig. 5 Plot of incident energy E_I versus scattering angle ϕ for a spin-wave stiffness of 300 meVÅ^2. The low-energy solution of Eq. (1) is plotted for Q = 0.05, 0.1 and 0.2 Å^{-1}. The corresponding energies are 0.75, 3 and 12 meV, respectively. The dashed lines extend to ϕ_{max} and E_I (ϕ_{max}), respectively. This figure shows the possible trade-off between incident energy and scattering angle for the chosen value of Q and the value of E determined by the choice of Q and D.

5. The instrument

The configuration proposed here is the low-angle flight path of a general-purpose high-resolution chopper spectrometer[11] being built at LANSCE. The spectrometer characteristics are given in Table 1. Neutrons emanate from a methane moderator and are monochromated by a 600-Hz phased chopper at a distance of 19 m before striking the sample at 20 m. The secondary flight path will extend a further 10 m for small scattering angles. In the epithermal regime, the incident energy resolution will be approximately 0.5%. This approach contrasts with that proposed by Egelstaff[3], in which a crystal monochromator is used to deflect neutrons out of the direct beam, the hope being that this will reduce the background.

6. Resolution considerations

In calculating the full resolution function for an experiment of this type, it is important to know the value of ϕ_Q, defined in Fig. 6 as the angle between $\underline{Q}$ and the incident wave-vector $\underline{k}_I$. ϕ_Q is given, by the sine and cosine rules respectively, as

$$\sin(\phi_Q) = \frac{k_F}{Q}\sin(\phi) \tag{16}$$

and

$$\cos(\phi_Q) = \frac{k_I^2 + Q^2 - k_F^2}{2k_IQ} \tag{17}$$

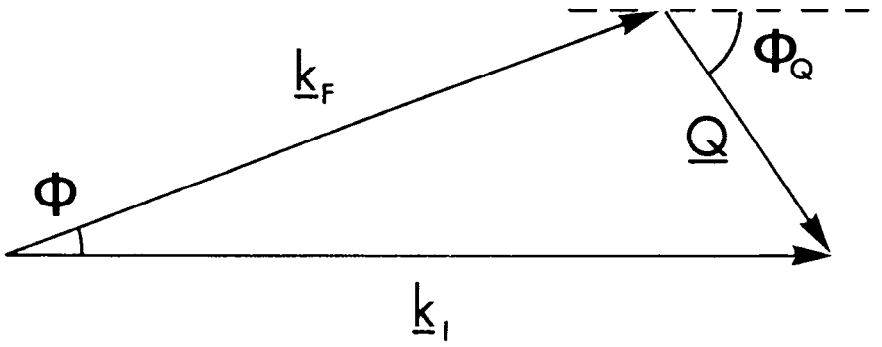

Fig. 6 A scattering triangle showing the definition of ϕ_Q.

The variation of ϕ_Q with E at fixed scattering angle is shown for one particular case in Fig. 7. For forward scattering ($\phi = 0$), $\phi_Q \rightarrow 0$ for neutron energy loss, while $\phi_Q \rightarrow 180^\circ$ for neutron energy gain. When $\phi = \phi_{max}$,

$$\sin(\phi_Q)^{\phi=\phi_{max}} = \sqrt{\frac{1}{2}\frac{Q^2}{2\varepsilon}} \tag{18}$$

For neutron energy loss, this means that ϕ_Q is less than 45°. Clearly, ϕ_Q can be greater than 45°, as shown in Fig. 7, but in that case one can reach the same energy transfer and Q using a lower incident energy.

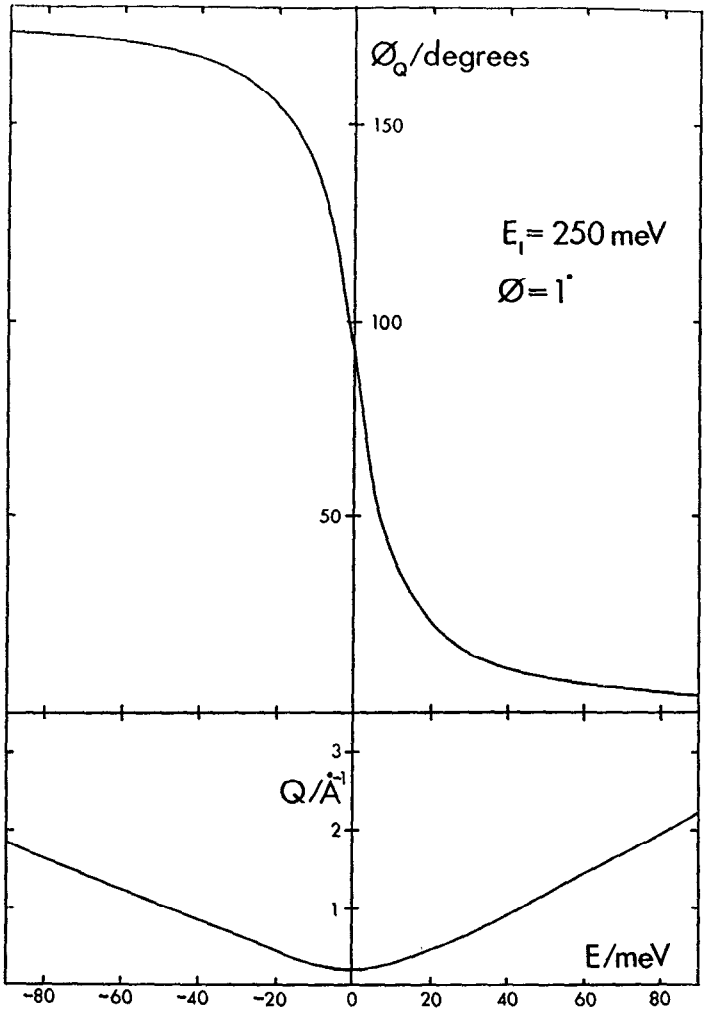

Fig. 7 The variation of (a) Q and (b) ϕ_Q within a time-of-flight scan at constant angle ϕ = 1° and constant incident energy, as might be observed in a single detector element in an experiment.

We have done a Monte-Carlo simulation of the instrument for the moderator, chopper and sample characteristics listed in Table 1. The sample thickness is ignored, as is

TABLE 1

Moderator-Chopper Distance	19 m
Chopper-Sample Distance	1 m
Sample-Detector Distance	4 m between 10° and 140°
	up to 10 m between -10° and +10°
Moderator	12.5 x 12.5cm^2 liquid methane
Source Repetition Frequency	12 or 24 Hz
Chopper Frequency	600 Hz
Chopper Diameter	10 cm
Chopper Slit Spacing	1 mm or more
Sample Size	up to 5 cm x 7.5 cm

appropriate for small-angle scattering. The detector is assumed to have circular symmetry about the straight-through beam and perfect angular and time resolution. Results for E_I = 250 meV and $\phi = 0.76^\circ$ are shown in Fig. 8. Clearly, both the energy and the Q resolution are sufficient for this case. Furthermore, the t and ϕ resolution is such that 2.5-cm-diam. position sensitive detectors at 10 m from the sample will easily have sufficient angular resolution for this experiment. It is also rather striking that there is some focusing (i.e., the resolution ellipse is oriented almost parallel to the dispersion surface for acoustic phonons) both in neutron energy loss and in neutron energy gain. In fact, the focusing is even more enhanced at larger Q values. This type of focusing has been discussed previously for Brillouin scattering experiments on triple-axis spectrometers[13]. As one would expect, the t and ϕ resolution is almost constant over this range of the scan, and the changes in Fig. 8 are mainly due to the fact that f_Q changes so dramatically, as in Fig. 7. In going from energy loss to energy gain, ϕ_Q goes from being parallel to $\underline{k}_I$ to being anti-parallel. Clearly, this type of focusing is not peculiar to chopper spectrometers or even constant-E_I instruments. It will occur on any instrument for which monochromation uncertainties dominate the resolution and when ϕ_Q is close to 0° or 180°. In principle, this focusing can be exploited in a Brillouin scattering measurement to improve the resolution without loss of intensity. However, the dispersion relation is almost tangential to the time-of-flight locus, so one needs to make constant-Q scans (or some other type of scan, for instance perpendicular to the dispersion curve) to exploit this focusing. This means that one would require rather good angular resolution, which would in turn permit reliable interpolation or two-dimensional rebinning.

7. Conclusions

We have discussed the kinematic constraints on doing neutron Brillouin scattering experiments: all the essential information is contained in the negative root of Eq. (1).

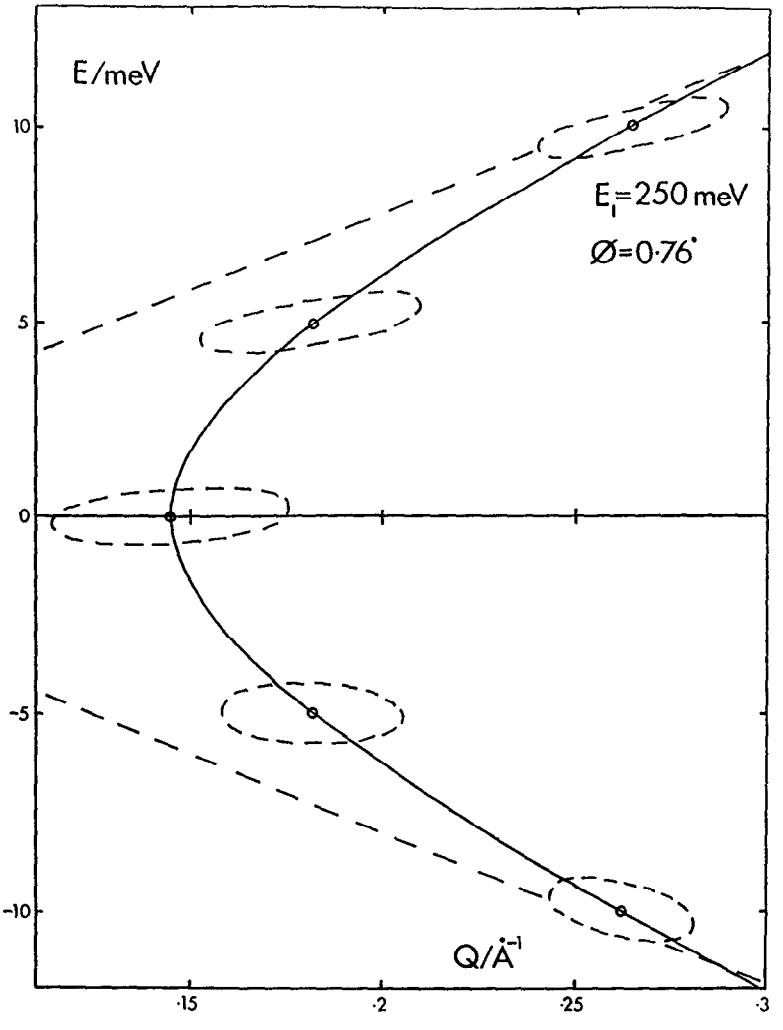

Fig. 8 The $Q_{||}$,E resolution for the proposed Los Alamos spectrometer with an incident energy of 250 meV and $\phi = 0.76°$. This corresponds to $v = 6000$ ms^{-1} and $Q = 0.3$ Å^{-1}, one of the special cases mentioned in the introduction. The solid curved line is the time-of-flight locus for these parameters and the straight dashed lines are the dispersion relations in neutron energy loss and gain for sound waves with $v = 6000$ ms^{-1}. The dashed ellipses represent contours at one standard deviation away from maximum assuming scattering from a delta-function in Q and E. The total energy widths are in good agreement with the standard analytic expressions given in Ref. 8. Note there is longitudinal resolution focusing both in energy loss and in energy gain. The physical origin of this effect is explained in the text.

For sound waves, the incident energies required are proportional to v^2 while the angular range is proportional to Q/v. For spin waves, the incident energies required are proportional to Q^2 while the angular range is independent of Q. Experiments on sound waves become progressively more difficult as Q decreases, because the scattering angle decreases. In contrast, those on spin waves become more difficult as Q increases because the incident energy increases very rapidly.

We have shown that the proposed LANSCE spectrometer will have sufficient E and Q resolution to perform such experiments and that there is some focusing, could be exploited in such experiments. Finally, the major unresolved question concerns background levels in such experiments, whether they be due to working close to the straight-through beam or to multiple scattering in the sample and its environment.

Acknowledgements

We are glad to acknowledge a number of fruitful discussions with Drs. J. M. Carpenter and R. Pynn. This work was supported, in part, by the division of Basic Energy Sciences of the U.S. Department of Energy.

Appendix: A Simple Graphical Proof that there are 2 physical roots to Equation 1 if $\varepsilon > Q^2$, but that only the positive root is physical for $\varepsilon < Q^2$.

Strictly speaking Eqn. 1 should be written with the $\cos^2\phi$ factor within the square root:

$$E_I = \frac{\hbar^2}{4m \sin^2\phi}\left\{(Q^2 + \varepsilon \sin^2\phi) \pm \sqrt{(Q^4 - \varepsilon^2 \sin^2\phi)\cos^2\phi}\right\} \tag{19}$$

This is the solution for E_I (or k_I), for given E, ϕ and Q. It is the properties of this equation that we shall now examine graphically.

Firstly, consider scattering triangles for which only the scattering angle ϕ and wave-vector transfer Q are fixed. The allowed incident wave-vectors $\underline{k}_I$ trace out a circle, as shown in Fig. 9a. Of course the energy transfer E increases as one moves around the circle in a clockwise fashion and the smaller circular arc (below the vector $\underline{Q}$) corresponds to scattering angle π-ϕ rather than ϕ.

Secondly, while remaing in the same space, consider scattering triangles for which only the energy transfer E and wave-vector transfer Q are fixed. From conservation of energy and conservation of momentum, it is straightforward to show that

$$\underline{k}_I \cdot \underline{Q} = \frac{1}{2}\left(\varepsilon + Q^2\right) \tag{20}$$

which is constant for given E and Q. In other words, the component of $\underline{k}_I$ parallel to

$\underline{Q}$ is constant, so that the allowed values of $\underline{k}_I$ lie on a straight line like that shown in Fig. 9b. Of course the scattering angle ϕ varies as one moves along this line.

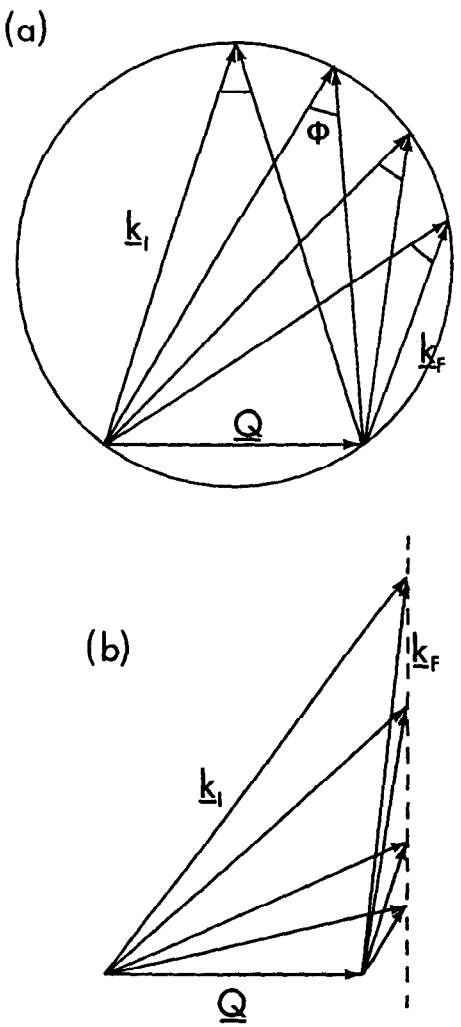

Fig. 9 (a) Allowed scattering triangles for constant Q and ϕ. $\underline{k}_I$ lies on a circle of radius $Q/(2\sin\phi)$. (b) Allowed scattering triangles for constant Q and E. $\underline{k}_I$ lies on the dashed line.

Now, the values of E_I given by Eqns. 1 and 19 are for constant E, Q and ϕ. These are then simply given by the intersections between the circular locus of Fig. 9a and the straight line of Fig. 9b. Fig. 10a shows a case where there are 2 allowed solutions, with scattering angle ϕ. In contrast, for the case shown in Fig. 10b, there are still 2 solutions, but the smaller triangle corresponds to a scattering angle of π -

ϕ. As $\underline{k}_I$ is smaller for this triangle, it corresponds to the negative "unphysical" root of Eqn. 1. The ambiguity within Eqns. 1 and 19 lies in the fact that both

$$\sin^2\phi = \sin^2(\pi - \phi) \tag{20}$$

and

$$\cos^2\phi = \cos^2(\pi - \phi) \tag{21}$$

so that Eqn. 19 is ambiguous between ϕ and $\pi - \phi$. In other words, it describes the full circle in Fig. 9a, and not just the upper arc corresponding to scattering angle ϕ.

Finally, the transition between a single physical root and two roots occurs for the right-angled triangle shown in Fig. 10c. By Pythagoras' Theorem, $Q^2 = k_I^2 - k_F^2$, but conservation of energy gives $\varepsilon = k_I^2 - k_F^2$, so the limiting condition is that $\varepsilon = Q^2$.

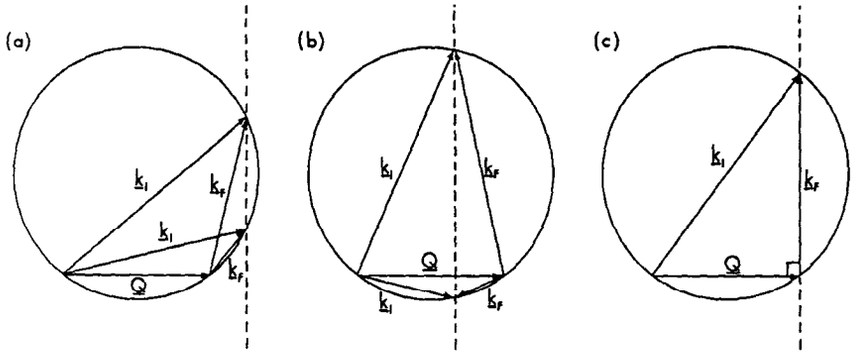

Fig. 10 Allowed scattering triangles for constant Q, ϕ and E, corresponding to the solutions of Eqs. (1) and (19). (a) for $\varepsilon > Q^2$, (b) for $\varepsilon < Q^2$ and (c) for $\varepsilon = Q^2$.

References

1. J. Skalyo and Y. Endoh, Phys. Rev. B7 (1973) 4670. N. A. Lurie, G. Shirane and J. Skalyo, Phys. Rev. B9 (1974) 2661. R. A. Robinson, J. D. Axe, A. I. Goldman, Z. Fisk, J. L. Smith and H. R. Ott, Phys. Rev. B33 (1986) 6488.
2. B. Dorner, Th. Plesser and H. Stiller, Discussions of the Faraday Society 43 (1967) 160. O. Söderström, J. R. D. Copley, J. -B. Suck and B. Dorner, J. Phys. F10 (1980) L151. J. Texeira, M. C. Bellissent-Funel, S. H. Chen and B. Dorner, Phys. Rev. Lett. 54 (1985) 2681.
3. P. A. Egelstaff in Proceedings of the Eighth meeting of ICANS, Oxford 8 - 12th July 1985, Rutherford Appleton Laboratory Report RAL-85-110 Vol II p. 546.
4. J. R. D. Copley, W. Gläser, W. S. Howells, D. L. Price, J. J. Rhyne, K. Sköld and C. Wagner, in Proceedings of Workshop on "Scientific Opportunities with Advanced Facilities for Neutron Scattering", Shelter Island, October 23-26 1984, CONF-8410256, p. 83.

5. W. Reichardt, in Proceedings of the Workshop on Neutron Scattering Instrumentation for SNQ, Maria Laach 3-5th September 1984, ed. R. Scherm and H. Stiller, Jülich Report Jül-1954, p. 312.
6. N. R. Bernhoeft, G. G. Lonzarich, D. McK. Paul and P. W. Mitchell, Physica 136B (1986) 443.
7. H. A. Mook and R. M. Nicklow, Phys. Rev. B7 (1973) 336.
8. P. W. Mitchell and D. McK. Paul, Phys. Rev. B32 (1985) 3272.
9. R. A. Robinson, Physica B156 (1989) 557.
10. M. W. Stringfellow, J. Phys. C1 (1968) 950.
11. J. M. Carpenter, K. Crawford, R. Kleb, C. -K. Loong, G. Ostrowski, D. L. Price, M. Nutter, R. Pynn, R. A. Robinson, R. N. Silver, J. M. Rowe, P. Sokol and A. D. Taylor, Los Alamos Report LA-UR-87-2582 (1987).
12. J. M. Carpenter, D. L. Price and N. J. Swanson, Argonne National Laboratory Report ANL-78-88 (1978) p. 78.
13. B. Dorner and H. H. Stiller, in "Instrumentation for Neutron Inelastic Scattering Research", I. A. E. A. Vienna (1970) p. 19.